Geomechanics and Engineering, *Vol. 18, No. 6 (2019) 639-650*
DOI: https://doi.org/10.12989/gae.2019.18.6.639

Viscous damping effects on the seismic elastic response of tunnels in three sites

Qiangqiang Sun[1], Jingshan Bo*[1] and Daniel Dias[2,3]

[1]*Institute of Disaster Prevention, Sanhe, China*
[2]*Laboratory 3SR, Grenoble Alpes University, Grenoble, France*
[3]*School of Automotive and Transportation Engineering, Hefei University of Technology, Hefei, China*

(Received December 18, 2017, Revised August 20, 2019, Accepted August 22, 2019)

Abstract. Time-domain commercial codes are widely used to evaluate the seismic behavior of tunnels. Those tools offer a good insight into the performance and the failure mechanism of tunnels under earthquake loading. Viscous damping is generally employed in the dynamic analysis to consider damping at very small strains in some cases, and the Rayleigh damping is commonly used one. Many procedures to obtain the damping parameters have been proposed but they are seldom discussed. This paper illustrates the influence of the Rayleigh damping formulation on the tunnel visco-elastic behavior under earthquake. Four Rayleigh damping determination procedures and three soil shear velocity profiles are accounted for. The results show significant differences in the free-field and in the tunnel response caused by different procedures. The difference is somewhat decreased when the soil site fundamental frequency is increased. The conventional method which consists of using solely the first soil natural mode to determine the viscous damping parameters may lead to an unsafe seismic design of the tunnel. In general, using five times site fundamental frequency to obtain the damping formulation can provide relatively conservative results.

Keywords: tunnel; seismic response; Rayleigh damping; small strain

1. Introduction

The seismic behavior of tunnels is of great concern since severe damages to tunnels are reported in recent earthquakes (Wang and Zhang, 2013, Yu *et al*. 2016). Among the existing methods, the numerical procedures are widely used to estimate the seismic performance of tunnels. To some extent, these approaches generally provide a good prediction of the tunnel behavior. However, some uncertainties still exist associated with the behavior of a tunnel under an earthquake loading which requires an analysis to consider the range of possible responses (Hardyniec and Charney 2015). Important uncertainties include the material constitutive relations, the soil-tunnel interaction, the input ground motions, the rock or soil properties, and the damping models. Many studies have been performed to understand the effect of the first three of type of uncertainties on the seismic behavior of tunnels (Cilingir and Madabhushi 2011, Hatzigeorgiou and Beskos 2010, Liu *et al*. 2015, Kontoe *et al*. 2011, Sedarat *et al*. 2009, Sevim 2013, Sun and Dias 2019a, b, Sun *et al*. 2016a, 2019, Zhang *et al*. 2017). However, little attention was given to the viscous damping effect.

By summarizing the recent numerical Round Robin on Tunnel Tests (*RRTT*), Bilotta *et al*. (2014) concluded that the different numerical predictions of five research groups (Amorosi *et al*. 2014, Conti *et al*. 2014, Gomes 2014, Hleibieh *et al*. 2014, Tsinidis *et al*. 2014), the uncertainty in the small strain viscous damping parameters had a significant effect, besides the constitutive models of soil. Manica *et al*. (2014) found that the damping models in *FLAC* had a significant impact on the free field response in Mexico city. Importantly, the effect was more evident in the elastic cases (Kwok, *et al*. 2007). Detailed investigations were done to discuss the influence of viscous damping (mostly focused on the Rayleigh damping) on the earthquake response of arch dams and other structures (Chen *et al*. 2012, Hardyniec and Charney 2015, Shih *et al*. 2016, Sun *et al*. 2016b, Sun and Bo 2017, Wang 2011, Zhang *et al*. 2009).

In this paper, first, a brief description of the Rayleigh damping model is presented, four damping determination procedures are described and selected. Then the comparison of those damping procedures effects on the seismic response of tunnels is performed in viscoelastic soil, a series of dynamic analysis of free-field and tunnels for three shear wave velocity profiles are carried out. In the end, the influence of the target damping ratio on the numerical results is also investigated, and the reasons which cause the differences are simply discussed.

2. Rayleigh damping

2.1 Presentation

In the non-linear analysis, the following dynamic equation of motion is solved

*Corresponding author, Professor
E-mail: bojingshan@163.com

ISSN: 2005-307X (Print), 2092-6219 (Online)

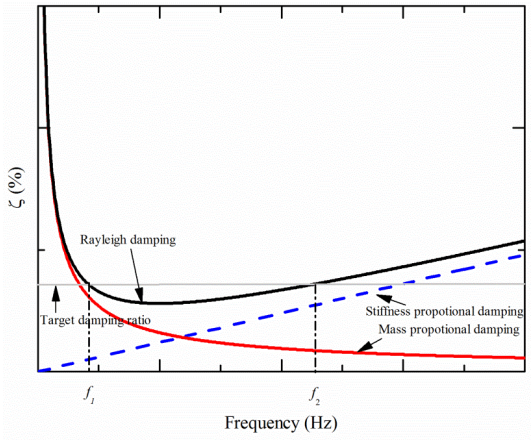

Fig. 1 Rayleigh damping

$$[M]\{\ddot{u}\} + [C]\{\dot{u}\} + [K]\{u\} = -[M]\{I\}\ddot{u}_g \quad (1)$$

where $[M]$ is the mass matrix; $[C]$ is the viscous damping matrix; $[K]$ is the stiffness matrix; $\{\ddot{u}\}$ is the vector of nodal relative acceleration; $\{\dot{u}\}$ is the vector of nodal relative velocities; and $\{u\}$ is the vector of nodal relative displacements; $\ddot{u}_g$ is the acceleration at the base of the soil column and $\{I\}$ is the unit vector.

There are generally two sources of damping (Priestley and Grant 2005). One is the hysteretic damping, associated with the area bounded by hysteretic stress-strain loops permits to dissipate energy. However, zero damping is usually encountered at small strain when the elastic model or the simple elastoplastic constitutive model is employed in the dynamic analysis, which is incompatible with the laboratory data (Carlton and Pestana 2016, Senetakis *et al*. 2015). It should be noted that only a small number of advanced and complex constitutive models can obtain satisfactory performances without using any additional mechanical damping, such as the bounding surface bubble model (Ni 2007). Additional viscous damping is necessary to overcome such a limitation, while the Rayleigh damping is widely adopted one.

The basic form of a frequency-dependent Rayleigh damping matrix is illustrated in Fig. 1, and can be expressed as follows

$$[C] = \alpha[M] + \beta[K] \quad (2)$$

where α and β are the mass-proportional and stiffness-proportional coefficients, respectively. The coefficients can be obtained according to the Eqs. (3) and (4)

$$\begin{Bmatrix}\alpha\\ \beta\end{Bmatrix} = \frac{2\zeta_{tar}}{\omega_i+\omega_j}\begin{bmatrix}\omega_i\omega_j\\ 1\end{bmatrix} \quad (3)$$

$$\zeta = \frac{1}{2}\left(\frac{\alpha}{\omega} + \beta\omega\right) \quad (4)$$

where ω_i and ω_j are the two parameters which ensure the frequency range, ζ_{tar} is the target damping ratio. ζ is the damping ratio used in the calculations.

There are two important issues for the Rayleigh damping (Hu, 2006): (1) the choice of the type of damping model; and (2) the method to obtain three key parameters: the target damping ratio ζ_{tar}; the matching frequencies f_1 and f_2, as shown in Fig. 1. For the type of damping model, the simplified and full Rayleigh damping matrix are mainly used, the extended Rayleigh damping is seldom used in practice. With regard to the target damping ratio, which is always based on the small strain damping or on the smallest value to obtain the stable solution, a constant damping ratio range between 1.5% to 5% for geo-material is often employed. For the matching frequencies, they are determined depending on the methods selected. Fig. 1 shows that for $f_1 < f < f_2$ the resulting damping ratio is less than the target damping ratio while for $f < f_1$ or $f > f_2$ the resulting damping ratio is significantly increased. The damping parameters determination procedures lead to different f_1 or f_2 values if no careful choice is made.

2.2 Methods to determine the damping

It is difficult to choose a reasonable frequency interval $[f_1, f_2]$ to cover the main frequency range of the input motions, especially when the ground motion frequency is much higher than f_2. In the geotechnical engineering field, many methods to determine the damping parameters are proposed.

For the hysteretic damping, the main methods are summarized as follows:

(1) Specimen tests, such as the resonant column test, the cyclic triaxial test, the bender element, and the cyclic simple shear test, etc. (Kokusho 1980, Lings and Greening 2001, Senetakis *et al*. 2015, Vucetic *et al*. 1998).

(2) Shaking table tests or centrifuge data (Brennan *et al*. 2005, Conti and Viggiani 2012, Li *et al*. 2013, Rayhani and Naggar 2008).

(3) Downhole array measurements (Mercado *et al*. 2015, 2017, Tasi and Hashash 2008, Groholski and Hashash 2013, Groholski *et al*. 2014) and the field measured data (Badsar *et al*. 2010, Guo *et al*. 2002).

(4) Element-scale numerical tests, such as a discrete element method (Dinesh *et al*. 2004, Tong and Wang 2015).

For the viscous (Rayleigh) damping, it mainly includes the following methods:

(1) Adopting the first natural mode of the soil (i.e., site fundamental frequency), and the characteristics of input ground motions (Hudson *et al*. 1994, Hashash and Park 2001, 2002, Kwok *et al*. 2007, Park and Hashash 2004, 2009, Tsai *et al*. 2014). The method is widely used in time-domain site response analysis, and the detailed introduction and comparison will be presented in the next section.

(2) Using the first natural mode only (Idriss *et al*. 1973). It is more commonly used in dynamic analysis, however, with great uncertainty and arbitrariness.

(3) Calibrating the viscous damping parameters using 1D free-field site response analysis program like *SHAKE*, *EERA* or *DEEPSOIL* (Amorosi *et al*. 2010, Visone *et al*. 2010). The equivalent-linear soil model is preliminary used to obtain the stiffness and damping parameters compatible with the effective deformation level expected during the earthquakes, then adopted those damping parameters in dynamic analysis. The process is complex and needs to be repeated if different input motions and soil properties are used.

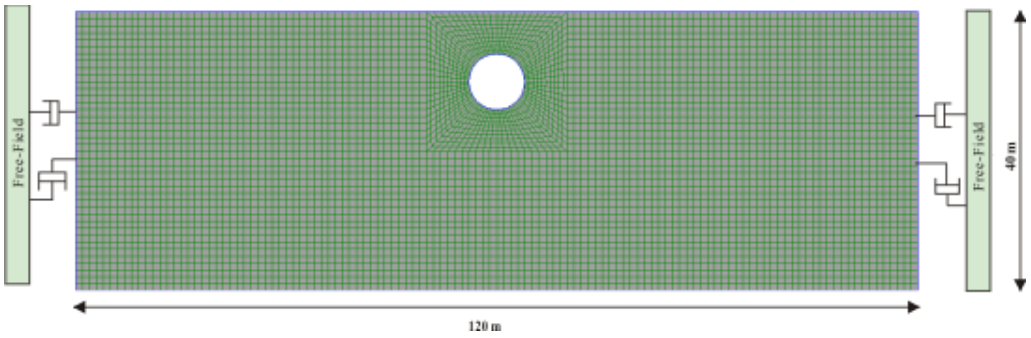

Fig. 2 Numerical model

2.3 Selection of the methods

Due to the limitation of the Rayleigh damping formulation, the defined frequency interval has a great effect on ground motion propagation. In current practice, the lower matching frequency f_1 is usually taken as the site fundamental frequency (1st natural mode); the difficulty is to determine the higher matching frequency f_2.

Several procedures were proposed to estimate the Rayleigh damping matrix. Idriss *et al*. (1973) only selected the site fundamental frequency to evaluate the seismic response of soil structures and implemented it in the code *QUAD4*. Then Hudson *et al*. (1994) improved this method, the odd-integer multiplier of the site fundamental frequency was selected to determine f_2 and was applied in the code *QUAD4M*. Park and Hashash (2001; 2002) compared the site response analysis using four soil modes (e.g., 1st, 2nd, 5th, 8th). They proposed an extended Rayleigh damping that accounted for the characteristics of input motions and the soil mass, then implemented it in the code *DEEPSOIL*. Kwok *et al*. (2007) compared three real sites seismic response and recommended the first mode site frequency and five times the site frequency can be used to achieve the damping matrix as a first approximation. Phillips and Hashash (2009) introduced an approach to construct a frequency-independent viscous damping formulation which reduced the overdamping at high frequencies. Tsai *et al*. (2014) suggested that the maximum among the predominant frequency, the mean frequency of the input motions and five times the site fundamental frequency can be selected to determine the higher frequency.

Based on the above study, in this article, a full Rayleigh damping is selected. The target damping ratio is adjusted to 5%, the f_1 is taken as the site fundamental frequency (abbreviated as SF hereafter) while the higher matching frequency f_2 are determined by four procedures, including:

(a) the site fundamental frequency (SF);
(b) the five times the site fundamental frequency (5SF);
(c) the predominant frequency of ground motions (PF);
(d) the mean frequency of ground motion (MF).

The site fundamental frequency can be estimated as follows (Kramer 1996)

$$SF = \frac{V_{se}}{4H} \tag{5}$$

$$V_{se} = \frac{H}{\sum(H_i/V_{si})} \tag{6}$$

where H is the total thickness of the soil, H_i is the thickness of the soil layer i; V_{se} is equivalent shear wave velocity of the soil, and V_{si} is the shear wave velocity of the soil layer i.

The mean frequency of ground motion, which can be calculated using Eq. (7)

$$MF = \frac{\int_{-\infty}^{+\infty} f \cdot S_{(f)} df}{\int_{-\infty}^{+\infty} S_{(f)} df} \tag{7}$$

where f is the frequency of ground motions, and $S_{(f)}$ is the power spectral density function of ground motions.

3. Numerical modeling

A two-dimensional numerical model is developed to simulate the seismic response of circular tunnels, using the finite difference program *FLAC* (Itasca, 2005) as presented in Fig. 2. Three different soil conditions are considered herein to study a wide range of site fundamental frequencies, as shown in Fig. 3.

The model considers the vertical propagation of horizontal shear waves, the input motion is one of the Friuli earthquake signal recorded at Tolmezzo station in 1976, as shown in Fig. 4. It is filtered to prevent frequency levels more than 15Hz in order to avoid the numerical distortion that may occur during the propagation of seismic waves inthe model.

The maximum elements size is calculated using Eq. (8), recommended by Lysmer and Kuhlemeyer (1969)

$$\Delta l \leq \frac{V_{smin}}{10 f_{max}} \tag{8}$$

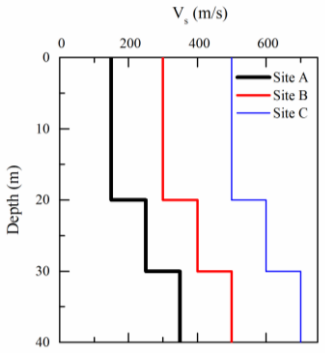

Fig. 3 Shear wave velocity profiles

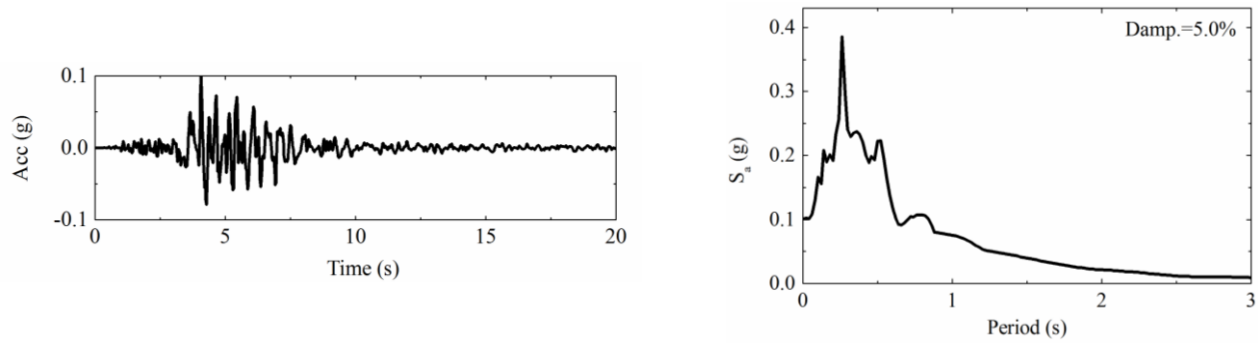

(a) (b)

Fig. 4 Input motion (a) acceleration time history and (b) spectral acceleration

Table 1 Parameters of site and tunnel

	Soil profile			Tunnel
	Site A	Site B	Site C	
Mass density, ρ (kg/m^3)	2000	2000	2000	2500
Shear wave velocity, *Vs* (m/s)	Variable with depth (see Fig 3)			-
Coefficient of earth pressure at rest, K_0	0.5	0.5	0.5	-
Poisson's ratio, ν	0.3	0.3	0.3	0.25
Target damping, *D* (%)	5	5	5	-
Fundamental site frequency, *SF* (Hz)	1.2	2.2	3.5	-
Radius, *r* (m)	-	-	-	4.0
Thickness, *t* (m)	-	-	-	0.6
Buried depth, *h* (m)	-	-	-	10
Elastic modulus, E_l (GPa)	-	-	-	35

where V_{smin} is the lowest shear-wave velocity, and f_{max} is the highest frequency of input motions. In this paper, the maximum element size adopted is equal to 1 m.

Other necessary parameters for the site and the tunnel are given in Table 1. A no-slip interface between soil and tunnel is considered in the model. For the dynamic calculation, the two vertical boundaries are defined as free-field boundary conditions, the velocity in the y-direction along the model base is fixed and the acceleration record is applied along this boundary.

4. Results

4.1 Accelerations

Fig. 5 presents a comparison of the PGA amplification factor variation along with soil profile for the three site conditions, as well as their Arias intensity (I_a) amplification factor. The Arias intensity gives a measure of the ground motion energy and is defined as

$$I_a = \frac{\pi}{2g}\int_0^t a^2(t)dt \quad (9)$$

where g is the gravitational acceleration, and t is the time.

The PGA or I_a amplification factor at a given depth is calculated as the ratio of the PGA or I_a at that depth to the PGA or I_a of the base motion. The PGA of the site A is amplified near the surface and then reduces the amplification at the depth between 10m and 20m. On the contrary, a continuous amplification appeared on the sites B and C. The different damping procedures used given the same variation trends. Variation of the I_a amplification factor along with soil depth is similar to the PGA ones, as shown in Fig. 5(b). For site A, a significant difference is observed for the PGA amplification factors and I_a. Taking 5SF as frequency f_2 results in the largest values for both PGA and I_a. Taking SF induces the minimum results, as mentioned above, this method is widely used in practice and leads to an underestimation. Similar results have been obtained in the previous studies (Kwok *et al*. 2007, Phillips and Hashash 2009, Tsai *et al*. 2014). The difference is decreased with the site fundamental frequency increases, a lower effect is observed in the case of site C.

The relative deviation of PGA and I_a for the three sites is presented in Fig. 6. The relative deviation is defined as

$$RD = \frac{PGA_i - 0.25\sum_1^4 PGA_i}{0.25\sum_1^4 PGA_i} \quad (10)$$

where PGA_i is the peak ground acceleration calculated by the damping method i, and the same formula is used for the RD of the Arias intensity.

In general, the relative deviations are large for low site fundamental frequency. The relative deviation is

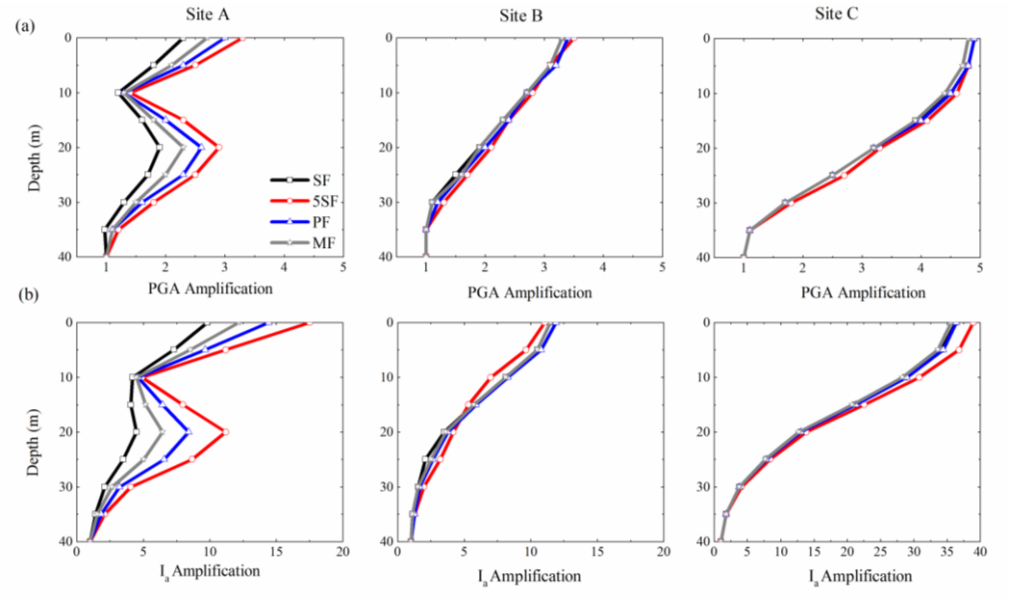

Fig. 5 Ground motion amplification factors in the free-field (a) *PGA* and (b) I_a

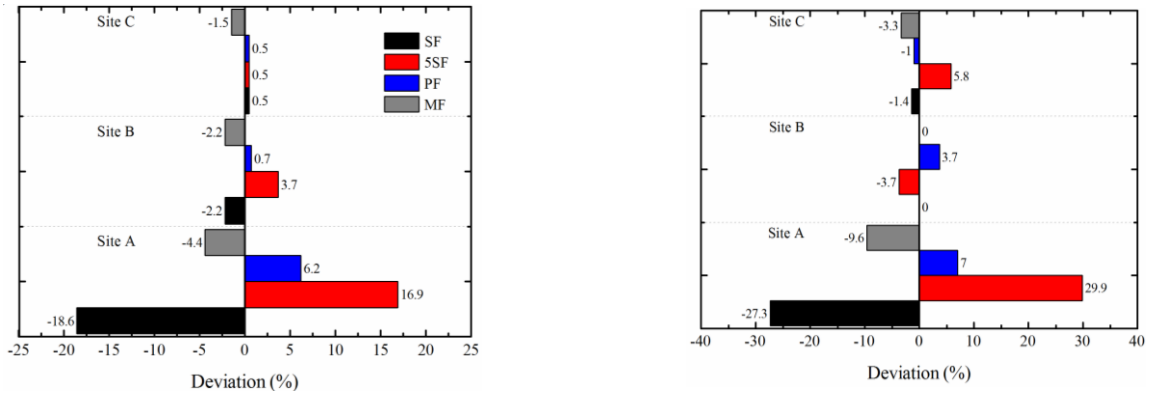

(a) (b)

Fig. 6 Relative deviations of ground surface motions (a) *PGA* and (b) I_a

decreased with the site fundamental frequency increases. For PGA of site A, the maximum RD is equal to 16.9% and the minimum RD is equal to -18.6%. For I_a, the maximum and minimum values are equal to 29.9%, and -27.3% respectively. It seems that the Rayleigh damping has a greater influence on the I_a than the PGA.

The surface ground accelerations calculated using four damping procedures are shown in Fig. 7, in terms of 5% damped surface acceleration response spectra and the Arias intensity time histories. For a specific site, the shape of the acceleration time histories with different four damping procedures are similar. Nevertheless, the shapes of acceleration time histories among the three sites are different. It shows that the site conditions strongly modify the frequency content of the input motions.

For the acceleration response spectra, the observed difference among the four damping procedures is significant for site A (period smaller than 0.3s), but the effect is negligible for sites B and C. For the site A, the maximum for the spectral values is obtained in the period between 0 and 0.3s when using 5SF as the frequency f_2. The minimum value occurs when SF is used as the frequency f_2. For site B, the choice of 5SF induces the largest spectral values in the period between 0 and 0.2s, and the smallest values in the period between 0.2 and 0.5s. The overestimation of the seismic response for smaller periods and the underestimation for larger periods may result from the lower or higher damping values for those frequencies interval, respectively. The reasons will be discussed in section 5.2. Finally, The site C fundamental frequency (SF=3.5Hz) coincides with the predominant frequency of the input motion and leads to the phenomenon of resonance. The behavior of the Arias intensities is similar, furthermore, it reaches the peak value fastly on much stiffer sites, whatever the type of the damping procedure used.

4.2 Internal forces

Fig. 8 illustrates the time histories of the axial force and bending moment at the right arch shoulder of the tunnel (θ=45°) during the earthquake. In order to distinguish the difference clearly, the internal forces only between the time range from 4 to 7s are presented. The maximum effects are included in this range. Similar to the acceleration time

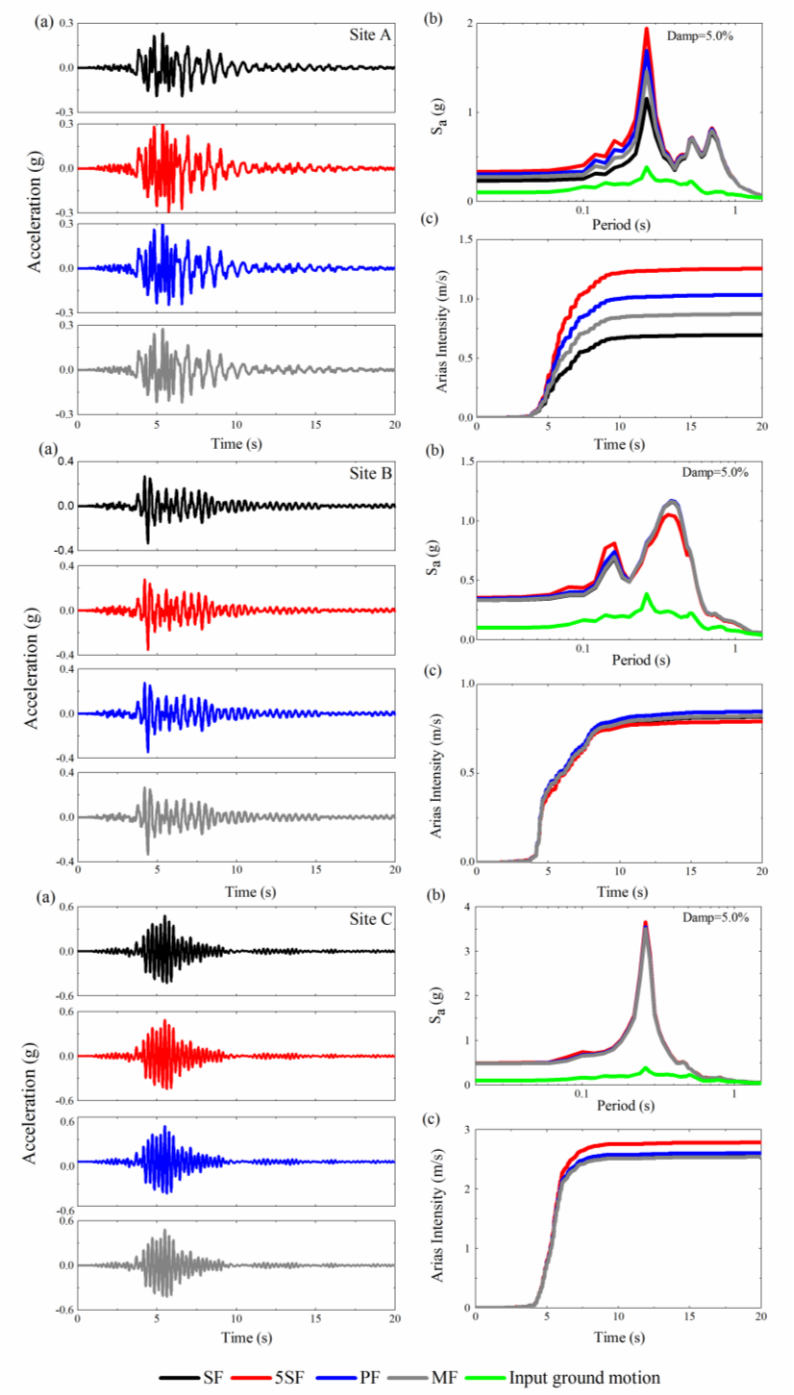

Fig. 7 Comparison of the surface motions for the three sites: (a) acceleration time histories, (b) 5%-damped spectral accelerations and (c) Arias intensity time histories

histories for a specific site, the shape of axial forces and bending moments time histories for the four different damping procedures are similar. Nevertheless, the evolution of the axial force and bending moment for site C are much more like the case of the free vibration due to the so-called phenomenon of resonance occurred.

The dynamic internal force increments along the perimeter of the tunnel are presented in Fig. 9. The dynamic internal force increments correspond to the earthquake-induced maximum internal forces during the earthquake. The results show that the damping methods do not change the distribution of the dynamic axial force increments and dynamic bending moment increments in the elastic response. The observed difference among the four damping methods are remarkable for site A for both axial forces and bending moments. A smaller influence is found on stiffer sites, especially for the case of the site C. The maximum internal force values are obtained using 5SF as the matching frequency, the minimum value occurred when using SF, and the ratio of the maximum value to the minimum value for axial force is nearly 1.5 while it is 1.4 for bending moment. Furthermore, the maximum dynamic bending moment and

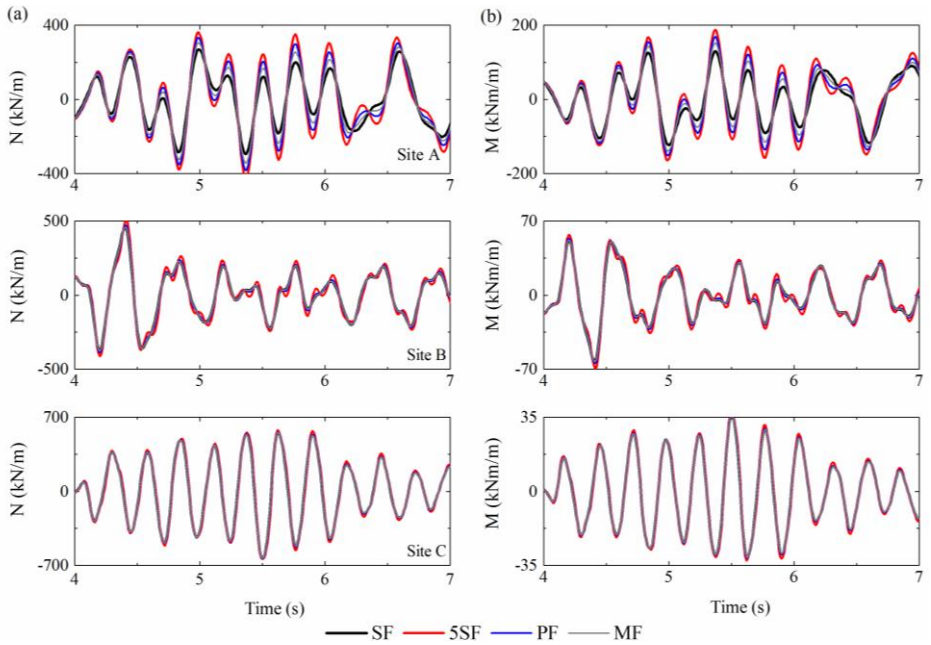

Fig. 8 Internal forces time histories at right arch shoulder: (a) dynamic axial force and (b) dynamic bending moments

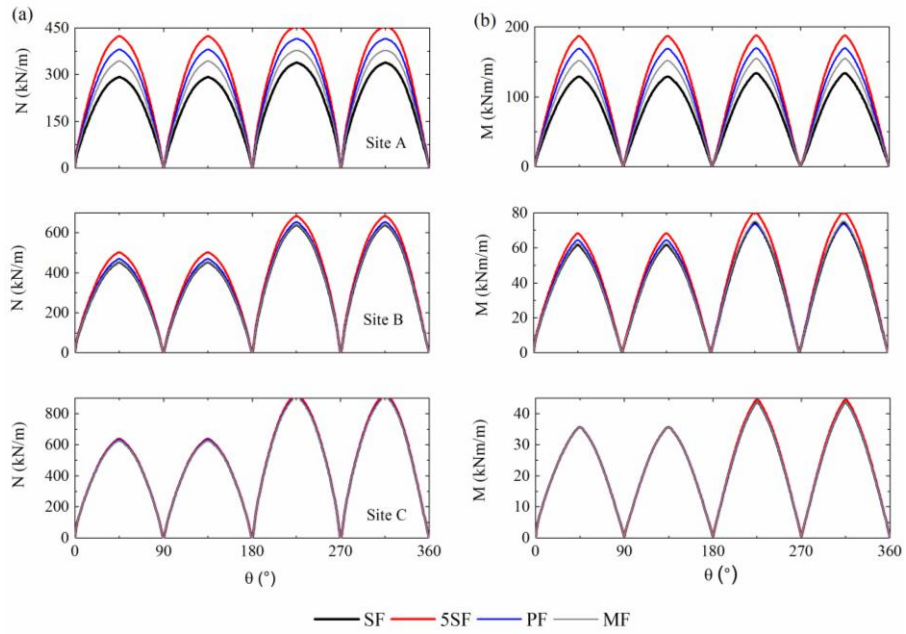

Fig. 9 Dynamic internal force increments along the perimeter of the tunnel: (a) axial force; (b) bending moments

the dynamic axial force occur near an angle of 45° (diagonal), the same with the analytical solutions (Bobet 2010, Park *et al*. 2009, Penzien 2000, Wang 1993).

As a general remark, the effect of the damping procedures on the tunnel response closely depend on the site condition. In order to quantify this influence, two dimensionless parameters: the internal force increment factor η and the flexibility ratio F (Peck *et al*. 1972) are used herein, defined as the following expressions

$$\eta = \frac{IF_{dyn}}{IF_{sta}} \tag{11}$$

where IF_{dyn} is the maximum dynamic internal force increment and IF_{sta} is the maximum static internal force.

$$F = \frac{E_m(1-\mu_l^2)r^3}{6E_l I(1+\mu_m)} \tag{12}$$

where E_m, μ_m are the elastic modulus, Poisson's ratio of the soil respectively; E_l, μ_l, r, I is the elastic modulus, Poisson's ratio, radius, and moment of inertia of the tunnel lining respectively.

The computed axial force and bending moment increment amplification factor are presented in Fig. 10. It should be noted that a decrease of the difference among the four damping procedures for a high flexibility ratio is observed for both axial forces and bending moments, although the internal force amplification factors are increased with the flexibility ratios increase. Using 5SF to

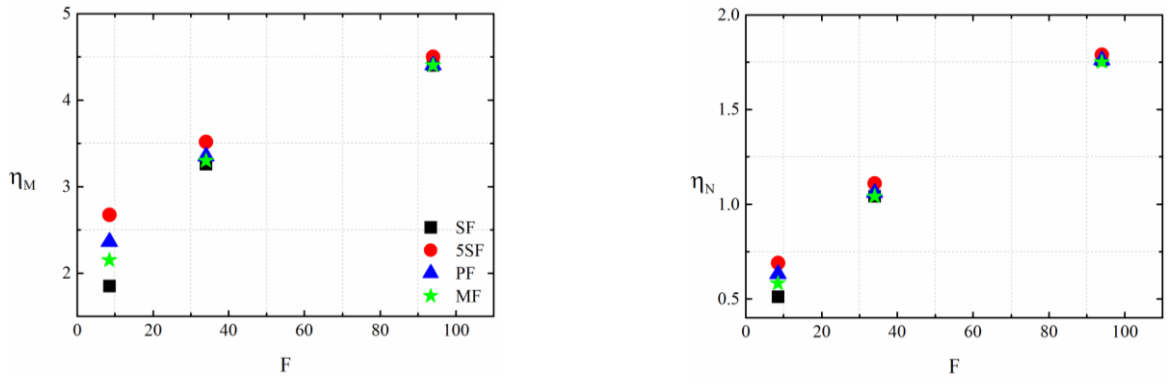

(a) (b)

Fig. 10 Dynamic internal force increments ratio η: (a) bending moments and (b) axial forces

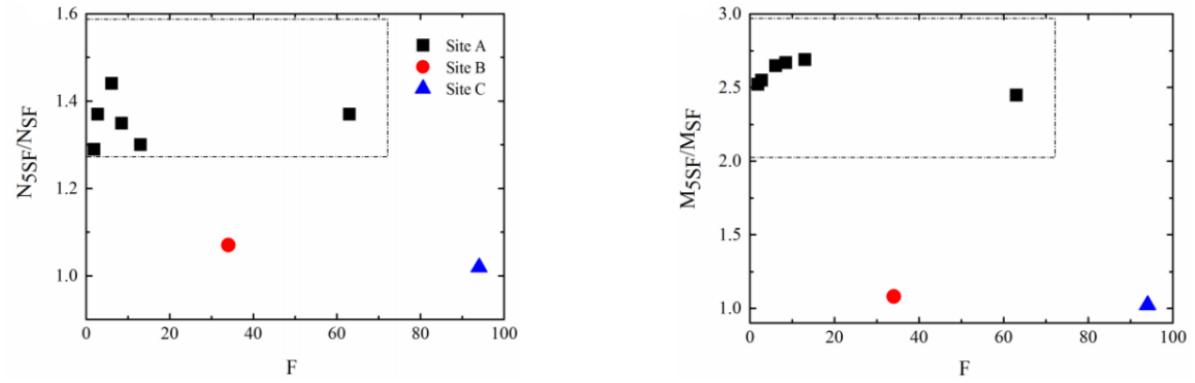

(a) (b)

Fig. 11 Comparisons of two damping models as a function of flexibility ratio: (a) axial forces and (b) bending moments

determine the damping parameters can result in a higher amplification factor. On the contrary, using SF induces the lower value.

The results indicate that the damping procedures can not modify the distribution of the dynamic internal force increments for an elastic analysis, but significant difference in terms of maximum dynamic internal force increments are obtained, especially for the site A. In fact, the flexibility ratio is also related to the diameter and thickness of the tunnel, the elastic modulus of soil and tunnel lining and Poisson's ratio of soil and tunnel lining (see Eq. (8)). In order to examine the damping determination procedures on the tunnel response with three thickness (0.2, 0.4 0.6 m) and three elastic moduli (15, 23, 32 GPa) of tunnel lining for a wide range of flexibility ratios. Only 5SF and SF for site A are investigated because this case leads to higher differences according to the above results.

The computed dynamic internal force increments ratios for the two damping procedures are presented in Fig. 11, as a function of the flexibility ratio. The results for sites B and C are also plotted. For the site A, the flexibility ratio is increased due to the thickness and the elastic modulus of the tunnel lining, the difference between the cases of 5SF and SF is not decreased, variation at a narrow range, near 1.4 in terms of axial force and bending moment. The tendency is different from the results in Fig. 10, it is worth remarking that the flexibility ratio in Fig. 11 depends on the mechanical parameters of the tunnel, while the flexibility ratio in Fig. 10 can significantly modify the characteristic of the input motions and of the Rayleigh damping matrix.

5. Discussion

5.1 Target damping ratio

As mentioned above, the target damping ratio is one of the three important parameters. In practice, the users usually take the small strain damping or the smallest damping to obtain a stable solution as the target damping ratio. In order to evaluate its effects, three target damping ratios are also selected to calculate the response on site A, the SF and 5SF are also chosen to obtain the Rayleigh damping matrix. It is noticed that the 10% and 20% target damping ratios are unrealistic and not employed in practice, the reason to select the higher values are only to distinguish clearly the tendency.

Fig. 12 and Fig. 13 compare the acceleration time histories, response spectra, and dynamic internal force increments, respectively. For peak ground accelerations and internal forces, the results are smaller at higher target damping ratio. The absolute difference of the results between two matching frequency determination procedures seems too small for the higher target damping ratio due to lower results are computed. The results of the present study have a good agreement with Kwok *et al*. (2007).

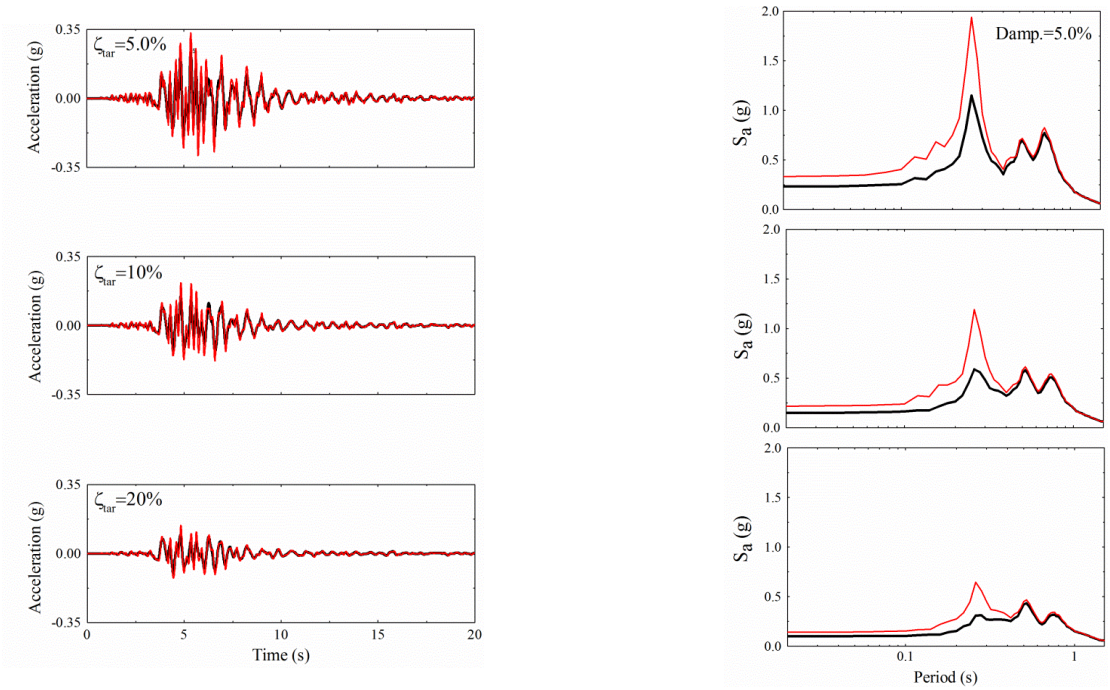

(a) (b)

Fig. 12 Surface ground motions in the free-field with three target damping ratio: (a) acceleration time histories and (b) spectral acceleration

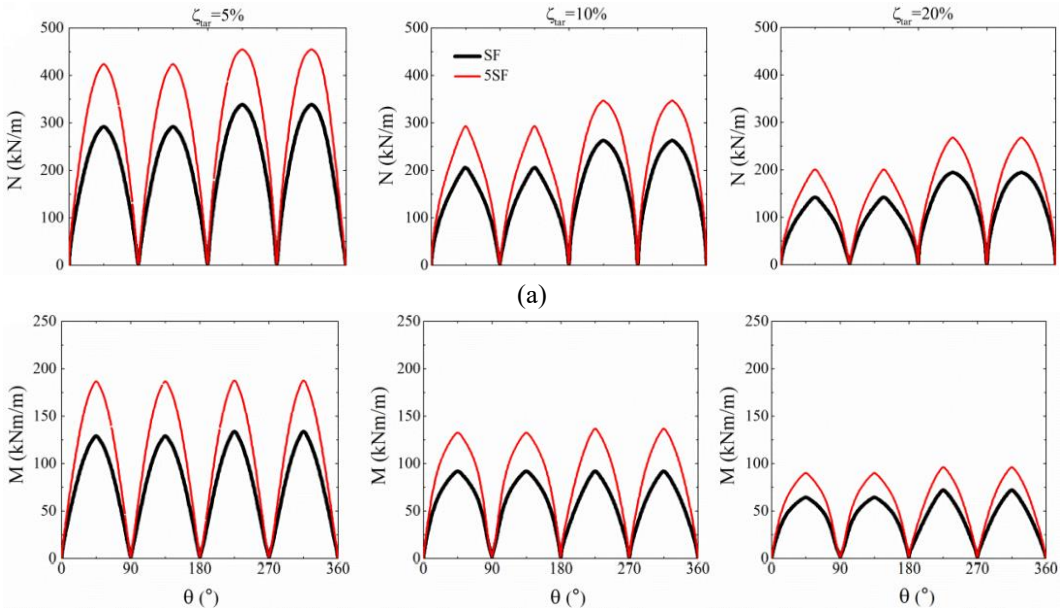

(a)

(b)

Fig. 13 Dynamic internal force increments along the perimeter of the tunnel at different target damping ratio: (a) axial force and (b) bending moments

5.2 Causal analysis

Fig. 14 shows the surface response spectra, the transfer function, the Fourier amplitude spectrum of the input motion and the effective damping ratio in the site A. The target damping ratio is taken equal to 5%, two damping procedures: SF and 5SF are chosen for analysis. Fig. 14 (c) shows that most components of the input ground motion are concentrated on the frequency range from PF to MF. Selecting SF to obtain the Rayleigh damping matrix, the effective damping ratio near MF is equal to 6.3%, higher than the target damping ratio (i.e., 5%) whereas 3.8% effective damping ratio is calculated by 5SF. The transfer functions of two damping ratios are calculated in the frequency-domain. Fig. 14 (b) shows the TF of 6.3% damping ratio and 3.8% damping ratio for comparison, the difference is significant after frequency greater than SF, lower TF means the smaller response. Furthermore, the soil

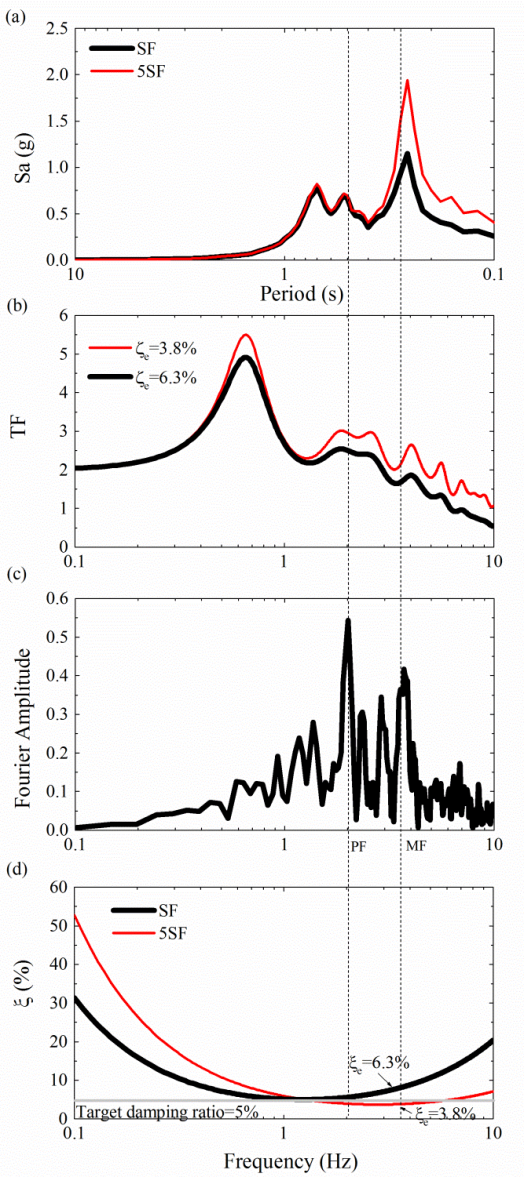

Fig. 14 Surface response spectrum, TF, Fourier amplitude spectrum of input motion and effective damping ratio in the site A

high modes are much easier to participate in the response in a soft site, but the first mode is in a dominant position in a much stiffer site (Phillips and Hashash 2009), this can enlarge the difference.

For the site A, five times site fundamental frequency is greater than the mean frequency and predominant frequency of the input ground motion, Tsai *et al*. (2014) recommend that a value of f_2 equal to 5SF should be chosen to obtain the damping parameters in this case, the results of this study validate their recommendations.

6. Conclusions

The effects of the Rayleigh damping on the seismic behavior of tunnels are studied using numerical modellings. The four damping procedures and three site conditions are considered. The following findings are observed:

A great influence is found for a softer site, but the impact is negligible for the much stiffer site. It seems that the difference caused by damping procedures deeply depend on the site conditions. When determining the Rayleigh damping parameters, the guideline to choose the two significant matching frequencies is to cover the main frequency component of the considered input motion. The conventional approach of using the first natural mode of the soil to determine the viscous damping parameters may not always result in conservative results; this may lead to an unsafe seismic design of the tunnel. Based on the results in the present study, considering simplicity in application, the five times site fundamental frequency is recommended and it provides a relatively reasonable result.

However, this paper does not consider the frequency characteristics of input motions, it may also underestimate the seismic response of the tunnel if the main frequency of input motions is much greater than the site fundamental

frequency. Furthermore, the Rayleigh damping effect in inelastic cases which accounting for the soil plasticity needs to be illustrated.

Acknowledgments

The authors gratefully thank the financial support of the National Natural Science Foundation of China (51208108).

References

Amorosi, A., Boldini, D. and Elia, G. (2010), "Parametric study on seismic ground response by finite element modeling", *Comput. Geotech.,* **37**(4), 515-528. https://doi.org/10.1016/j.compgeo.2010.02.005.

Amorosi, A., Boldini, D. and Falcone G. (2014), "Numerical predication of tunnel performance during centrifuge dynamic tests", *Acta Geotechnica*, **9**(4), 581-596. https://doi.org/10.1007/s11440-013-0295-7.

Badsar, B.A., Schevenels, M., Haegeman, W. and Degrande, G. (2010), "Determination of the material damping ratio in the soil from SASW tests using the half-power bandwidth method", *Geophys. J. Int.*, **182**(3), 1493-1508. https://doi.org/10.1111/j.1365-246X.2010.04690.x.

Bilotta, E., Lanzano, G., Madabhushi, S.P.G. and Silvestri, F. (2014), "A numerical round robin on tunnels under seismic actions", *Acta Geotechnica*, **9**(4), 563-579. https://doi.org/10.1007/s11440-014-0330-3.

Bobet, A. (2010), "Drained and undrained response of deep tunnels subjected to farfield shear loading", *Tunn. Undergr. Sp. Technol.*, **25**(1), 21-31. https://doi.org/10.1016/j.tust.2009.08.001.

Brennan, A.J., Thusyanthan, N.I. and Madabhushi, S.P.G. (2005), "Evaluation of shear modulus and damping in dynamic centrifuge tests", *J. Geotech. Geoenviron. Eng.*, **131**(12), 1488-1497. https://doi.org/10.1061/(ASCE)1090-0241(2005)131:12(1488).

Carlton, B.D. and Pestana, J.M. (2016), "A unified model for estimating the in-situ small strain modulus of clays, silts, sands, and gravels", *Soil Dyn. Earthq. Eng.*, **88**, 345-355. https://doi.org/10.1016/j.soildyn.2016.01.019.

Chen, D.H., Du, C.B., Yuan, J.W. and Hong, Y.W. (2012), "An investigation into the influence of damping on the earthquake response analysis of a high arch dam", *J. Earthq. Eng.*, **16**(3), 329-349. https://doi.org/10.1080/13632469.2011.638697.

Cilingir, U. and Madabhushi, S.P.G. (2011), "A model study on the effects of input motion on the seismic behavior of tunnels", *Soil Dyn. Earthq. Eng.*, **31**(3), 452-462. https://doi.org/10.1016/j.soildyn.2010.10.004.

Conti, R., Viggiani, G.M.B. and Perugini, F. (2014), "Numerical modelling of centrifuge dynamic tests of circular tunnels in dry sand", *Acta Geotechnica*, **9**(4), 597-612. https://doi.org/10.1007/s11440-013-0286-8.

Dinesh, S.V., Sitharam, T.G. and Vinod, J.S. (2004), "Dynamic properties and liquefaction behavior of granular materials using discrete element method", *Current Sci.*, **87**(10), 1379-1387.

Gomes, R.C. (2014), "Numerical simulation of the seismic response of tunnels in sand with an elastoplastic model", *Acta Geotechnica*, **9**(4), 613-629. https://doi.org/10.1007/s11440-013-0287-7.

Guo, X., Wong, Y.L. and Yuan, Y.F. (2002), "Estimation of damping ratio of soil sites using microtremor", *Earthq. Eng. Eng. Vib.*, **1**(1), 45-49. https://doi.org/10.1007/s11803-002-0006-0.

Groholski, D.R. and Hashash Y.M.A. (2013), "Development of an inverse analysis framework for extracting dynamic soil behavior and pore pressure response from downhole array measurements", *Int. J. Numer. Anal. Meth. Geomech.*, **37**(12), 1867-1890. https://doi.org/10.1002/nag.2172.

Groholski, D.R., Hashash, Y.M.A. and Matasovic, N. (2014), "Learning of pore pressure response and dynamic soil behavior from downhole array measurements", *Soil Dyn. Earthq. Eng.*, **61**, 40-56. https://doi.org/10.1016/j.soildyn.2014.01.018.

Hardyniec, A. and Charney, F. (2015), "An investigation into effects of damping and nonlinear geometry models in earthquake engineering analysis", *Earthq. Eng. Struct. Dyn.*, **44**, 2695-2715. https://doi.org/10.1002/eqe.2604.

Hashash, Y.M.A. and Park, D. (2001), "Non-linear one-dimensional seismic ground motion propagation in the Mississippi embayment", *Eng. Geol.*, **62**(1-3), 185-206. https://doi.org/10.1016/S0013-7952(01)00061-8.

Hashash, Y.M.A. and Park, D. (2002), "Viscous damping formulation and high frequency motion propagation in non-linear site response analysis", *Soil Dyn. Earthq. Eng.*, **22**(7), 611-624. https://doi.org/10.1016/S0267-7261(02)00042-8.

Hatzigeorgiou, G.D. and Beskos, D.E. (2010), "Soil-structure interaction effects on seismic inelastic analysis of 3-D tunnels", *Soil Dyn. Earthq. Eng.*, **30**(9), 851-861. https://doi.org/10.1016/j.soildyn.2010.03.010.

Hleibieh, J., Wegener, D. and Herle, I. (2014), "Numerical simulation of a tunnel surrounded by sand under earthquake using a hypoplastic model", *Acta Geotechnica*, **9**(4), 631-640. https://doi.org/10.1007/s11440-013-0294-8.

Hudson, M., Idriss, M. and Beikae, M. (1994), "User manual for QUAD4M: A computer program to evaluate the seismic response of soil structures using finite element procedures and incorporating a compliant base," University of California, Berkeley, California, U.S.A.

Hu, Y.X. (2006), *Earthquake Engineering*, Seismological Press, Beijing, China.

Idriss, I.M., Lysmer, J. and Hwang, R. (1973), "QUAD4: A computer program for evaluating the seismic response of soil structures by variable finite element procedures," University of California, Berkeley, California, U.S.A.

Itasca. (2005), *Software Manual of FLAC Version5.0*, Itasca Consulting Group.

Kontoe, S., Zdravkovic, L., Potts, D.M. and Menkiti, C.O. (2011), "On the relative merits of simple and advanced constitutive models in dynamic analysis of tunnels", *Geotechnique,* **61**(10), 815-829. http://dx.doi.org/10.1680/geot.9.P.141.

Kokusho, T. (1980), "Cyclic triaxial test of dynamic soil properties for wide strain range", *Soil. Found.*, **20**(2), 45-60. https://doi.org/10.3208/sandf1972.20.2_45.

Kramer, S.L. (1996), *Geotechnical Earthquake Engineering*, Prentice-Hall, Upper Saddle River, New Jersey.

Kwok, A.O.L., Stewart, J.P., Hashash, Y.M.A., Matasovic, N., Pyke, R., Wang, Z.Z. and Yang, Z.H. (2007), "Use of exact solution of wave propagation problems to guide implementation of nonlinear seismic ground response analysis procedures", *J. Geotech. Geoenviron. Eng.*, **133**(11), 1385-1398. https://doi.org/10.1061/(ASCE)1090-0241(2007)133:11(1385).

Li, Z., Escoffier, S. and Kotronis, P. (2013), "Using centrifuge tests data to identify the dynamic soil properties: Application to Fontainebleau sand", *Soil Dyn. Earthq. Eng.*, **52**, 77-87. https://doi.org/10.1016/j.soildyn.2013.05.004.

Lings, M.L. and Greening, P.D. (2001), "A novel bender/extender element for soil testing", *Geotechnique*, **51**(8), 713-717.

Liu, X.R., Li, D.L., Wang, J.B. and Wang, Z. (2015), "Surrounding rock pressure of shallow-buried bias tunnels under earthquake", *Geomech. Eng.*, **9**(4), 427-445. https://doi.org/10.12989/gae.2015.9.4.427.

Lysmer, J. and Kuhlemeyer, R.L. (1969), "Finite dynamic model for infinite media", *J. Eng. Div.*, **95**(4), 859-877.

Manica, N., Ovando, E. and Botero, B. (2014), "Assessment of damping models in FLAC", *Comput. Geotech.*, **59**, 12-20. https://doi.org/10.1016/j.compgeo.2014.02.007.

Ni, B. (2007), "Implementation of a bubble model in Flac and its application in dynamic analysis," Ph.D. Thesis, University of Auckland, Auckland, New Zealand.

Park, D. and Hashash, Y.M.A. (2004), "Soil damping formulation in nonlinear time domain site response analysis", *J. Earthq. Eng.*, **8**(2), 249-274.

Park, K.H., Tantayopin, K., Tontavanich, B. and Owatsiwong, A. (2009), "Analytical solution for seismic-induced ovaling of circular tunnel lining under no-slip interface conditions: A revisit", *Tunn. Undergr. Sp. Technol.*, **24**(2), 231-235. https://doi.org/10.1016/j.tust.2008.07.001.

Peck, R.B., Hendron, A.J. and Mohraz, B. (1972), "State of the art of soft ground tunnelling", *Proceedings of the Rapid Excavation and Tunnelling Conference*, Chicago, Illinois, U.S.A., June.

Penzien, J. (2000), "Seismically induced racking of tunnel linings", *Earthq. Eng. Struct. Dyn.*, **29**(5), 689-691. https://doi.org/10.1002/(SICI)1096-9845(200005)29:5%3C683::AID-EQE932%3E3.0.CO;2-1.

Phillips, C. and Hashash, Y.M.A. (2009), "Damping formulation for nonlinear 1D site response analyses", *Soil Dyn. Earthq. Eng.*, **29**(7), 1143-1158. https://doi.org/10.1016/j.soildyn.2009.01.004.

Priestley, M.J.N. and Grant, D.N. (2005), "Viscous damping in seismic design and analysis", *J. Earthq. Eng.*, **9**(Spec2), 229-255.

Rayhani, M.H.T. and Naggar, M.H.E. (2008), "Dynamic properties of soft clay and loose sand from seismic centrifuge tests", *Geotech. Geol. Eng.*, **26**(5), 593-602. https://doi.org/10.1007/s10706-008-9192-5.

Sedarat, H., Kozak, A., Hashash, Y.M.A., Shamsabadi, A. and Krimotat, A. (2009), "Contact interface in seismic analysis of circular tunnels", *Tunn. Undergr. Sp. Technol.*, **24**(4), 482-490. https://doi.org/10.1016/j.tust.2008.11.002.

Senetakis, K., Anastasiadis, A. and Pitilakis, K. (2015), "A comparison of material damping measurements in resonant column using the steady-state and free-vibration decay method", *Soil Dyn. Earthq. Eng.*, **74**, 10-13. https://doi.org/10.1016/j.soildyn.2015.03.009.

Sevim, B. (2013), "Assessment of 3D earthquake response of the Arhavi Highway tunnel considering soil-structure interaction", *Comput. Concrete*, **11**(1), 51-61. https://doi.org/10.12989/cac.2013.11.1.051.

Shih, J.Y., Thompson, D.J. and Zervos, A. (2016), "The effect of boundary conditions, model size and damping models in the finite element modeling of a moving load on track/ground system", *Soil Dyn. Earthq. Eng.*, **89**, 12-27. https://doi.org/10.1016/j.soildyn.2016.07.004.

Sun, Q.Q., Bo, J.S., Sun, Y.W. and Zhang, Z.P. (2016a), "A state-of-the-art review of seismic response analysis of tunnels", *World Earthq. Eng.*, **32**, 159-169.

Sun, Q.Q., Bo, J.S., Li, X.B. and Wang, X. (2016b), "Comparative study of viscous damping formulation in time-domain site response analysis", *Earthq. Eng. Eng. Dyn.*, **36**, 171-179.

Sun, Q.Q. and Bo, J.S. (2017), "Effect of Rayleigh damping matrix on seismic response analysis of deep soft site", *Chin. Earthq. Eng.*, **39**, 506-510.

Sun, Q.Q. and Dias, D. (2019a), "Assessment of stress relief during excavation on the seismic tunnel response by the pseudo-static method", *Soil Dyn. Earthq. Eng.*, **117**, 384-397. https://doi.org/10.1016/j.soildyn.2018.09.019.

Sun, Q.Q. and Dias, D. (2019b), "Seismic behavior of circular tunnels: Influence of the initial stress state", *Soil Dyn. Earthq. Eng.*, **126**, 105808. https://doi.org/10.1016/j.soildyn.2019.105808.

Sun, Q.Q., Dias, D. and Sousa, L.R. (2019), "Impact of an underlying soft soil layer on tunnel lining in seismic conditions", *Tunn. Undergr. Sp. Technol.*, **90**, 293-308. https://doi.org/10.1016/j.tust.2019.05.011.

Tong, L. and Wang, Y.H. (2015), "DEM simulation of shear modulus an damping ratio of sand with emphasis on the effects of particle number, particle shape, and aging", *Acta Geotechnica*, **10**(1), 117-130. https://doi.org/10.1007/s11440-014-0331-2.

Tsai, C.C. and Hashash, Y.M.A. (2008), "A novel framework integrating downhole array data and site analysis to extract dynamic soil behavior", *Soil Dyn. Earthq. Eng.*, **28**(3), 181-197. https://doi.org/10.1016/j.soildyn.2007.06.008.

Tsai, C.C., Park, D. and Chen, C.W. (2014), "Selection of the optimal frequencies of viscous damping formulation in nonlinear time-domain site response analysis", *Soil Dyn. Earthq. Eng.*, **67**, 353-358. https://doi.org/10.1016/j.soildyn.2014.10.026.

Tsinidis, G., Pitilankis, K. and Trikalioti, A. D. (2014), "Numerical simulation of round robin numerical test on tunnels using a simplified kinematic hardening model", *Acta Geotechnica*, **9**, 641-659. https://doi.org/10.1007/s11440-013-0293-9.

Visone, C., Bilotta, E. and Magistris, F.S.D. (2010), "One-dimensional ground response as a preliminary tool for dynamic analyses in geotechnical earthquake engineering", *J. Earthq. Eng.*, **14**(1), 131-162. https://doi.org/10.1080/13632460902988950.

Vucetic, M., Lanzo, G. and Doroudian, M. (1998), "Damping at small strains in cyclic simple shear test", *J. Geotech. Geoenviron. Eng.*, **124**(7), 585-594. https://doi.org/10.1061/(ASCE)1090-0241(1998)124:7(585).

Wang, J.N. (1993), *Seismic Design of Tunnels: A State-of-the-Art Approach*, Parsons, Brinckerhoff, Quade and Douglas Inc., New York, U.S.A.

Wang, J.T. (2011), "Investigation of damping in arch dam-water-foundation rock system of Mauvoisin arch dam", *Soil Dyn. Earthq. Eng.*, **31**, 33-44.

Wang, Z.Z. and Zhang, Z. (2013), "Seismic damage classification and risk assessment of mountain tunnels with a validation for the 2008 Wenchuan earthquake", *Soil Dyn. Earthq. Eng.*, **45**, 45-55. https://doi.org/10.1016/j.soildyn.2012.11.002.

Yu, H.T., Chen, J.T., Bobet, A. and Yuan, Y. (2016), "Damage observation and assessment of the Longxi tunnel during the Wenchuan earthquake", *Tunn. Undergr. Sp. Technol.*, **54**, 102-116. https://doi.org/10.1016/j.tust.2016.02.008.

Zhang, C.H., Pan, J.W. and Wang, J.T. (2009), "Influence of seismic input mechanisms and radiation damping on arch dam response", *Soil Dyn. Earthq. Eng.*, **29**(9), 1282-1293. https://doi.org/10.1016/j.soildyn.2009.03.003.

Zhang, B., Wang, X., Zhang, J.S. and Meng, F. (2017), "Three-dimensional limit analysis of seismic stability of tunnel face with quasi-static method", *Geomech. Eng.*, **13**(2), 301-318. https://doi.org/10.12989/gae.2017.13.2.301.

GC